Is Kinetic Molecular Sieving of Hydrogen Isotopes Feasible?

ARTICLE *in* THE JOURNAL OF PHYSICAL CHEMISTRY C · MARCH 2008

Impact Factor: 4.77 · DOI: 10.1021/jp8015358 · Source: OAI

Is Kinetic Molecular Sieving of Hydrogen Isotopes Feasible?

A. V. Anil Kumar and Suresh K. Bhatia*

Division of Chemical Engineering, The University of Queensland, Brisbane - 4072, Australia

Received: February 20, 2008; Revised Manuscript Received: May 7, 2008

We investigate the possibility of kinetic molecular sieving of hydrogen isotopes by studying their dynamical properties in the one-dimensional channels of microporous aluminophosphate $AlPO_4$-25 at low temperatures. We use transition state theory as well as molecular dynamics simulations, using an effective quantum potential obtained via the Feynman−Hibbs path integral formalism. With the help of the free energy profile and barrier determined using the Widom particle insertion method, we demonstrate that transition state theory offers an effective and convenient method to determine self-diffusion coefficients, showing excellent agreement with those obtained from molecular dynamics simulations. Quantum-effect-induced kinetic molecular sieving, in which the heavier isotope (deuterium) diffuses faster than the lighter hydrogen, is observed at low temperature, consistent with our simulation results for narrow window zeolite-ρ, and experimental evidence with 3 Å carbon molecular sieve in the recent literature. The free energy profile provides insight into this remarkable counterintuitive behavior, showing that at sufficiently low temperature the free energy barrier for diffusion is smaller for deuterium than hydrogen and exhibits inverse temperature dependence. These findings suggest low-temperature kinetic molecular sieving of hydrogen isotopes as an attractive route for their separation.

1. Introduction

The molecular level description of the structure and dynamics of fluids confined in microporous solids is usually based on classical mechanics. Although generally successful in many contexts where quantum effects are small, at low temperatures quantum effects can become increasingly important, especially for light molecules such as hydrogen and helium.[1] Quantum effects are thus noticeable, and their relevance for understanding most of the static and transport properties is now starting to be quantitatively assessed. For example, it has been shown that quantum effects act to lower the transition rate for diffusion of hydrogen and deuterium on a Pd(111) surface relative to classical predictions. This in turn causes an inverse isotope effect in which the heavier isotope, deuterium, has a faster rate than hydrogen.[2] Voth and co-workers,[3,4] as well as Miura et al.,[5] used centroid molecular dynamics to study the influence of quantum effects on the structure and dynamics of hydrogen and helium. For these simple light fluids, when confined to narrow pores at sufficiently low temperatures, quantum effects associated with the positional uncertainty are expected to substantially modify the equilibrium and dynamical properties from the classical description and can lead to intriguing effects in confined fluids. For example, molecular hydrogen exhibits a strong isotope effect in equilibrium adsorption at low temperatures, in which deuterium is adsorbed more strongly than hydrogen. This was first proposed by Beenaker et al., while investigating quantum effects for hard spheres confined in hard cylindrical pores.[6] Subsequently, Sholl and co-workers confirmed this equilibrium isotope effect in carbon nanotubes using analytical methods and path integral Monte Carlo simulations.[7,8] Since then there have been several computational and experimental investigations on confined hydrogen isotopes that have corroborated the existence of this phenomenon.[9–11]

Quantum effects on the dynamics of hydrogen in confined systems are found to be even more striking, where a crossover of the transport diffusivities occur at low temperatures. This leads to a reversal of kinetic selectivity in which the heavier deuterium diffuses faster than lighter hydrogen provided the pore dimensions of the confining medium are sufficiently small. This was first proposed by us while studying the diffusion of hydrogen and deuterium in zeolite-ρ at low temperatures using molecular dynamics simulations.[12,13] The experimental support for this observation came soon after, from Zhao et al.,[14] who observed that deuterium diffuses faster than hydrogen in porous carbon molecular sieves with micropore dimension of 0.546 nm and 0.566 nm, which are similar to the window dimensions in zeolite-ρ. More recently, Chu et al. have investigated the equilibrium and dynamical adsorption of hydrogen and deuterium in various mesoporous and microporous materials at 77 K[15] and reported that although the rate of adsorption for hydrogen is larger than that of deuterium in mesoporous materials, this order reverses in small micropores. The ratio of rate of adsorption of deuterium to that of hydrogen was found to have a maximum at a pore dimension of about 0.5 nm. These results validate our prediction of the reversal of kinetic selectivity in sufficiently narrow confinements, due to quantum effects. A combination of this equilibrium and kinetic selectivity, as is effective in membrane-based molecular sieving, is proposed as a more attractive technique for hydrogen isotope separation, compared to the more energetically demanding conventional cryogenic distillation route.

We report here our investigations on the dynamical properties of hydrogen and deuterium in $AlPO_4$-25 using transition state theory (TST) and molecular dynamics (MD) simulations, and demonstrate that TST offers an attractive and insightful route to determine the transport coefficients that is also much less computationally demanding than MD. The paper is organized as follows: In Section 2 we provide the details of the structure of $AlPO_4$-25, which is used as the model microporous host in these investigations. The methodology used is described in

* Author to whom all correspondence should be addressed. E-mail: s.bhatia@eng.uq.edu.au.

10.1021/jp8015358 CCC: $40.75
Published on Web 07/08/2008

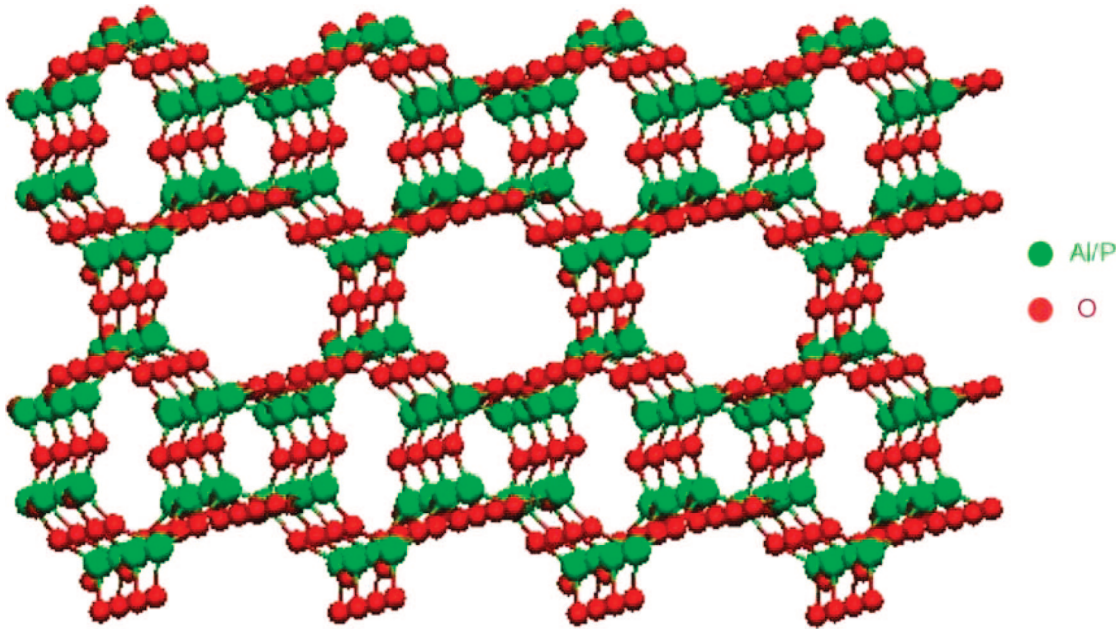

Figure 1. (2 × 2 × 2) unit cells of $AlPO_4$-25. The coordinates of the atoms are taken from ref.[12]

Section 3. The main results will be outlined in Section 4, and we present our conclusions in Section 5.

2. Structure of $AlPO_4$-25

A series of open framework aluminophosphates were first prepared by Wilson et al. in the 1980s using organic amines as the templates in a hydrothermal synthesis system.[12] These are denoted by $AlPO_4$-*n*. These materials typically possess three-dimensional (3D) frameworks built up from alternating AlO_4 and PO_4 tetrahedra. $AlPO_4$-25 is obtained by calcination from $AlPO_4$-21 through a topotactic transformation. $AlPO_4$-25 has a one-dimensional (1D) channel along the *z*-axis, formed by eight-membered rings, and has unit cell parameters $a = 9.4489$ Å, $b = 15.2028$ Å, and $c = 8.4084$ Å, with the crystal structure falling in the space group *Acmm*. The atomic coordinates and structure reported by Richardson et al. have been used in the simulations.[16] Figure 1 depicts (2 × 2 × 2) unit cells of $AlPO_4$-25.

3. Methodology

To incorporate quantum corrections to the dynamics for H_2 and its isotopes, we employ the Feynman−Hibbs (F−H) variational approach,[17] as in our previous investigations.[12,13] The F−H potential is obtained from the path integral quantum partition function for a canonical ensemble of particles. We use the effective quantum potential shown in eq 1,[12]

$$U_{FH}(r) = U(r) + \frac{\beta\hbar^2}{24\mu}\left[U''(r) + \frac{2U'(r)}{r}\right] + \frac{\beta^2\hbar^4}{1152\mu^2}\left[\frac{15U'(r)}{r^3} + \frac{4U'''(r)}{r} + U''''(r)\right] \quad (1)$$

obtained upon expanding the FH potential around the classical path, with fluctuations retained up to the fourth order. It must be noted that this fourth order expansion is done on the vector space **r.** This formulation improves upon any classical interaction potential, such as the Lennard−Jones model, by taking into account quantum features. Here $U(r)$ is the classical potential and $U'(r)$, $U''(r)$, etc. are the first, second, and higher derivatives of $U(r)$; $\hbar$ is Plank's constant; $\beta = 1/k_BT$; and μ is the reduced mass. The second and third term on the right-hand side (rhs) of eq 1 represent perturbations to the classical potential, with an inverse dependence on temperature (T) as well as the reduced mass (μ). Consequently, quantum corrections will be more significant for light mass molecules such as H_2 and at low temperatures. We have previously shown that these corrections impose two important but competing effects on the classical potential.[12] First, they reduce the depth of the energy minimum by reducing the energy barrier for diffusion. Second, the position at which the potential becomes zero shifts toward a higher value. This effectively increases the diameter of the molecule, which in turn results in an increase in the energy barrier for diffusion. Thus, these two adjustments to the potential have opposing effects, which compete in modifying the diffusion. Our previous investigations have shown that the increase in effective diameter has a more significant effect than the reduction in the depth of the energy minimum, for fluids confined in narrow pores where pore dimensions are very similar to molecular dimensions,[12,13] as a result of which the transport coefficient in the confined space reduces below that expected from the classical description.

TABLE 1: Lennard−Jones Interaction Parameters, σ and ε, for Fluid−Fluid and Fluid−Solid Interactions Used in TST and MD Simulations

	σ (nm)	ε/k_B (K)
H_2−H_2	0.2782	38.7
O−O	0.2644	165.02

The interaction potentials between the sorbate−sorbate and sorbate−host particles are modeled by the 12−6 Lennard−Jones potential. The interaction parameters ε and σ are the same as those used in our previous investigations.[13] These are given in Table 1. Following the general practice,[18] the interaction between the sorbate molecules and Al/P atoms in the solid framework is not considered, as these atoms are well inside the framework and are sufficiently distant from the sorbate molecules. A cutoff distance of 1.2 nm was used in evaluating all pair potentials.

As discussed above, we have used dynamically corrected transition state theory and MD simulations in this investigation. In transition state theory, diffusion is considered as an activated

process in which the particle jumps between the valleys in the potential energy surface through a barrier that is significantly higher than thermal energy k_BT. The thermally activated escape of the particle through the potential barrier from a state A can be estimated by transition state theory following the rate expression of eq 2.[19]

$$k_{TST} = \frac{k_B T}{h} \frac{Q^*}{Q_A} e^{-E^*/k_B T} \quad (2)$$

Here, the top of the potential barrier denotes the transition state. E^* is the height of the potential barrier above the potential well; Q_A and Q^* are the partition functions in the well and the transition state, respectively; and the temperature (T) provides the driving force for the escape over the barrier. This equation ignores the nonreactive recrossings of the transition state, that is, it does not take into account of the trajectories that recross the potential energy barrier immediately after a crossing. One can then write a phenomenological correction to the transition state theory by introducing a transmission coefficient, in which a great deal of the dynamical information is condensed.[20]

$$k = \kappa k_{TST} \quad (3)$$

This transmission coefficient can be easily calculated using MD simulations. To calculate k_{TST}, one may rewrite eq 2 as shown in eq 3.

$$k_{TST} = \frac{k_B T}{h} e^{-\Delta F/k_B T} \quad (4)$$

Here, ΔF is the free energy difference between the transition state and the energy well. This can be reframed as shown in eq 5,[21]

$$k_{TST} = \frac{1}{2} \nu \frac{\int_{TS} e^{-U/k_B T} \, dS}{\int_A e^{-U/k_B T} \, dV} \quad (5)$$

where ν is the average velocity of the molecule at the transition state, and the integrals of the Boltzmann factor are over the volume of the reactant cage and the surface area of the transmission state. We used a simple numerical integration in a cylindrical coordinate system to evaluate the surface and volume integrals in eq 5. The diffusion coefficient (D) was then calculated from k_{TST} by eq 6.[22]

$$D_{TST} = (\delta^2/2)k \quad (6)$$

Here, δ is the distance between two energy minima separated by an energy barrier, the factor 2 in the denominator arises from the fact that the diffusion in $AlPO_4$-25 is essentially 1D, that is, along the c-axis.

Molecular dynamics simulations have been performed in the canonical ensemble. We have used ($10 \times 5 \times 10$) unit cells of $AlPO_4$-25 with 250 H_2/D_2 molecules, with periodic boundary conditions in all three dimensions. This corresponds to a sorbate density of 0.5 particles per unit cell. At this density, sorbate interaction is negligible and the results correspond to the low-density values. The equations of motions are integrated using a fifth order Gear predictor−corrector algorithm with a time step of 1 fs. In our simulations, we adopted a rigid host framework, neglecting the lattice vibrations. Although there have been many investigations reported in the literature studying the influence of lattice vibrations on transport properties of confined fluids, their importance remains inconclusive.[23–25] Moreover, the temperatures at which we have done our calculations are very low, so the lattice vibrations can be safely ignored. The temperature of the system is maintained constant by means of a Gaussian thermostat.[26] Self and transport diffusivities are computed by using the Einstein formula (eq 7).

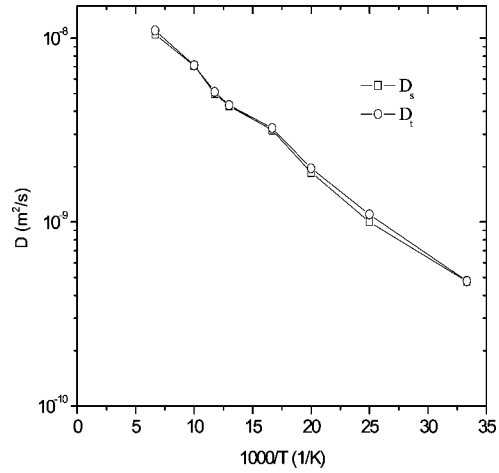

Figure 2. Self and transport diffusivities of classical H_2 versus inverse temperature obtained from molecular dynamics simulations. Circles correspond to self-diffusion coefficients and squares to transport diffusion coefficients. At this low density, both are expected to have similar values.

$$D_{MD} = \langle r^2(\Delta t) \rangle / 2\Delta t \quad (7)$$

Here $\langle r^2(\Delta t) \rangle$ corresponds to the average of single-particle mean squared displacement in the case of self-diffusivity and to the average of the center-of-mass mean square displacement in the case of transport diffusivity. At the low density at which we carried out the simulations, it is expected that both self and transport diffusivities should be the same. Typical simulation runs correspond to 500 ps of equilibration, followed by 5 ns of production run during which the equilibrium and dynamic properties are calculated.

4. Results and Discussion

At the low density chosen for the simulations, adsorbate−adsorbate interactions are negligible and the self and transport diffusivities are expected to be similar. This was indeed verified by the MD simulations, as illustrated in Figure 2, which depicts the self and transport diffusivities of classical H_2 obtained from MD simulations at different temperatures. The excellent match between the two diffusivities confirms the insignificance of the interaction between the sorbate molecules at very low densities. This equivalence of the two transport coefficients at low density was also observed in other cases, that is, quantum H_2, as well as classical and quantum D_2.

Figure 3 depicts the diffusivities of H_2 and D_2 at different temperatures, obtained using the classical LJ potential and the quantum FH potential. Open symbols correspond to the classical self-diffusivities and closed ones to the quantum values. Solid lines connect values obtained from transition state theory and the dashed lines to those obtained from MD simulations. The MD simulations also allow us to assess dynamical corrections to the transition state theory. For this, we analyzed the MD trajectories in detail and examined possible instances of re-crossings. These were found to be negligible for our system, in agreement with Beerdsen et al.[27] where the transmission coefficient was found to be very close to unity at low sorbate density. Consequently, we have taken the transmission coefficient to be unity in our calculations. From the figure it is clear that agreement between the two methods (MD and TST) is good,

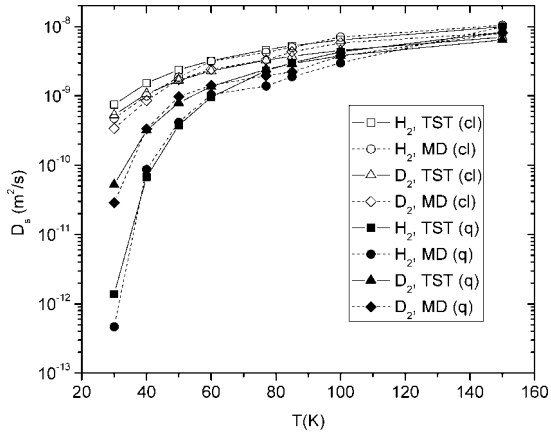

Figure 3. Classical and quantum self-diffusivities of H_2 and D_2 obtained from TST and MD simulations plotted against inverse of temperatures. Open symbols correspond to classical values and closed symbols to their quantum counterparts. The solid lines connect the values obtained from TST and dashed lines those obtained from MD simulations. The lines are provided as guides to the eye.

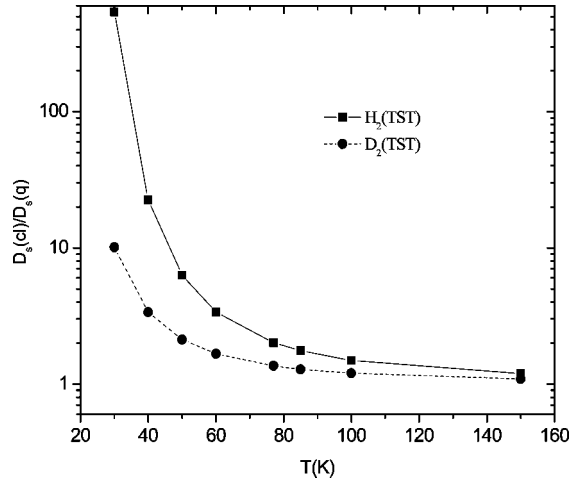

Figure 4. The ratio of classical diffusivity to quantum diffusivity of H_2 and D_2, obtained using TST calculations.

with some deviation at the lowest temperature, that is, at 30 K. At this temperature, the rate of diffusion, that is, the jumping of molecules over the energy barrier, becomes a rare event and may not be accurately captured by MD simulations. However, the excellent agreement between TST and MD at other temperatures validates use of the former technique for calculating diffusivities.

At high temperatures, the classical and quantum values do not appreciably differ, as seen from the clustering of points at 150 K. From eq 1, it is clear that quantum correction term in the potential is inversely dependent on the temperature. Thus, at high temperatures this correction to the potential is very small and effectively leads to similar values for diffusion coefficients for the classical and quantum cases. However, at low temperatures the correction to the potential becomes larger, and the classical and quantum values of diffusion coefficient begin to differ. With reduction in the temperature this difference increases, as shown by the ratios between the classical and quantum values in Figure 4. Although we have shown only the ratios from TST calculations, those from the MD simulations follow the same pattern. Another feature to be noted is that the ratio between classical and quantum diffusivities is higher for H_2 compared to D_2. Again, this is due to the quantum correction in eq 1, which is inversely dependent on reduced mass of the

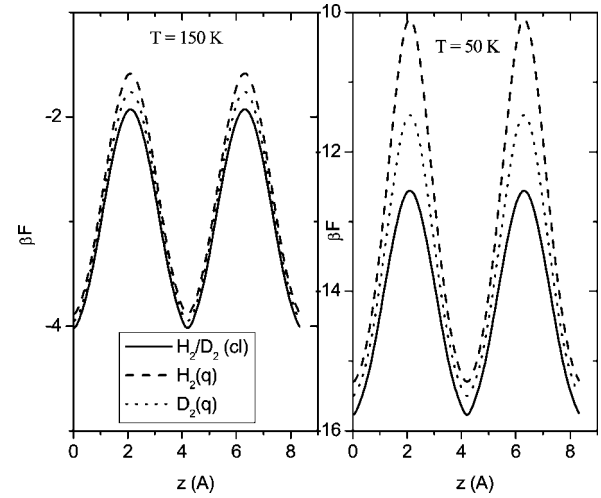

Figure 5. Classical and quantum free energy profile of diffusion for H_2 and D_2 at (a) 150 K, and (b) 50 K. It should be noted that classical free energy profiles for hydrogen and deuterium are identical.

molecule. Thus, the lighter molecule will feel the quantum effects more than the heavier molecule, and the decrease in diffusivity is therefore larger for H_2.

To probe the underlying course for the decrease in diffusivity when quantum corrections to the intermolecular interaction are considered, we have calculated the free energy along the reaction path, which is along the *c*-axis of $AlPO_4$-25 in this case. To estimate the free energy, we have carried out Monte Carlo (MC) simulations in the NVT ensemble at the density used in MD simulations (0.5 molecules per unit cell). During the MC simulations, we used Widom particle insertion method to obtain the free energy.[28] The Widom particle insertion method uses a probe particle that is inserted at random positions to measure the energy required or achieved due to the insertion of the particle in the system. This energy is mapped into the reaction coordinates to obtain the free energy profile according to eq 8.

$$\beta F = -\ln\langle e^{-\beta \Delta U}\rangle \tag{8}$$

At high loadings the Widom particle insertion method is known to give erroneous results,[29] but at the low density at which we have carried out the calculations it is known to be satisfactory. Figure 5 depicts the free energy profile of classical H_2/D_2 and quantum H_2 and D_2 at two different temperatures. It must be noted that the classical H_2 and D_2 are indistinguishable except for the mass and give the same free energy profile. However, in the quantum case, the interaction potentials differ due to the quantum correction term in the interaction potential [c.f. eq 1], which gives rise to different free energy profiles. At high temperature, the differences between the quantum and classical free energy profiles are very small, and the molecules have to surmount essentially the same free energy barrier to move from one potential well to another. Thus, the diffusivities do not show a significant difference at high temperatures, say at 150 K. However, at 50 K the differences between the classical and quantum energy profiles are significant.

The quantum molecule has to surmount a higher energy barrier while diffusing compared to its classical counterpart, as a result of which the quantum values of diffusivities are smaller than the classical values. From Figure 5 it is clear that at low temperature the difference in the free energy barrier between the classical and quantum cases is more significant than at higher temperatures, so that the ratio between classical and quantum diffusivities increases as we move down the temperature scale.

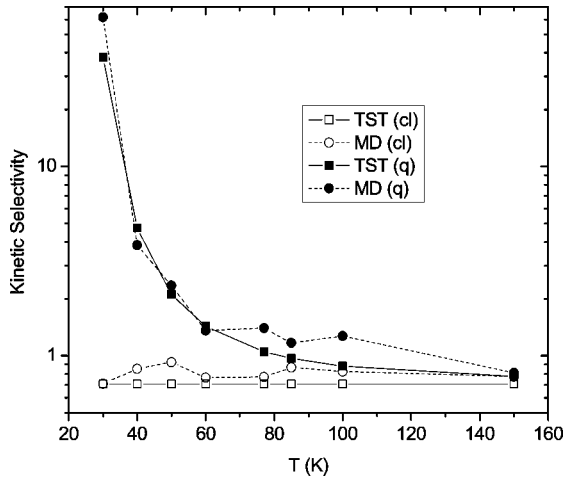

Figure 6. Kinetic selectivity of D_2 over H_2 in $AlPO_4$-25 versus temperature, obtained from TST and MD simulations. Open symbols correspond to classical values and closed symbols to quantum values. Squares correspond to TST values and circles to MD results.

Further, the free energy barrier is greater for quantum H_2 than quantum D_2, and this leads to a higher reduction in the diffusivity of quantum H_2 from its classical value compared to that of D_2. This results in a higher ratio for H_2 in Figure 4 compared to D_2.

A dramatic and counter-intuitive consequence of having a higher difference between the classical and quantum diffusivities for H_2 is that at sufficiently low temperatures the heavier D_2 diffuses faster than lighter H_2. This is the quantum mediated reverse kinetic selectivity effect that was first reported by us based on MD simulations of H_2 and D_2 in zeolite-ρ[12,13] and subsequently experimentally supported by Zhao et al.[14] Here again, we observe this reverse kinetic sieving in $AlPO_4$-25. Both TST and MD predict the crossover temperature at which the diffusivity of D_2 becomes larger than that of H_2 to be around 110−120 K, which is comparable to the value of 94 K predicted for zeolite-ρ.[13] At lower temperatures, this reverse kinetic sieving increasingly becomes more significant, which is attributable to an increase in the free energy barrier for diffusion on reduction in temperature. Thus, the H_2 molecule, being of lighter mass, will be severely restricted at low temperatures, which reduces its diffusivity. This leads to a higher kinetic selectivity for D_2 at sufficiently low temperature.

Figure 6 depicts the kinetic selectivity, which is the ratio of diffusivity of D_2 to that of H_2, for the classical and quantum cases. The solid line corresponds to TST values and the dashed line to MD values. In the classical case, the MD-based selectivity is less than unity at all temperatures. TST gives a value of 0.71 at all temperatures, which is the square root of the mass ratio, as expected. The MD results, although not constant, fluctuate around this value, due to the statistical error involved in computing the diffusivities. The quantum selectivity is around unity at 150 K and increases as the temperature decreases. Here also, the TST and MD results are in good agreement with each other, with some deviation at 30 K. The kinetic selectivity reaches a value of ∼50 at 30 K in the TST and ∼70 in the case of MD. Such high values suggest the possibility of H_2/D_2 separation by low-temperature kinetic molecular sieving using a microporous membrane comprised of a suitable narrow pore size material. Although the material investigated here ($AlPO_4$-25) is not suited for this purpose because of the occurrence of single file diffusion in its 1D channels, membranes comprised of other materials such as zeolite-ρ or carbon molecular sieves may be appropriate for this purpose. Further, although these selectivities are considerably lower than other estimates[7−10] for quantum sieving of hydrogen isotopes, it should be noted that these earlier results were purely based on equilibrium separation rather than kinetic separation. A combination of the kinetic and equilibrium selectivity will provide high flux selectivity, which is pertinent to membrane separation. From a practical point of view it is the latter that will be more appropriate when processing large quantities.

5. Conclusions

We have carried out transition state theory calculations and MD simulations to study the quantum effects on diffusion of hydrogen isotopes in $AlPO_4$-25. The quantum correction to the classical potential is incorporated through the F−H path integral formalism. The results from TST and MD simulations are in good agreement with each other and demonstrate that the diffusivities of hydrogen and deuterium decrease from their classical values when quantum corrections are incorporated. The free energy profile along the reaction coordinate is obtained from NVT Monte Carlo simulations using the Widom particle insertion method for both classical and quantum cases, showing an increase in the energy barrier for both hydrogen and deuterium when the quantum effect is considered. This behavior explains the reduction in quantum diffusivities compared to their classical counterparts. Further, quantum-mediated reversal of kinetic selectivity in which the heavier deuterium starts diffusing faster than lighter hydrogen in $AlPO_4$-25 is observed, as reported earlier in MD simulations for zeolite-ρ and in experiments of different nanoporous materials. This property may have applications in the development of improved and more economical methods for separating hydrogen isotopes. Most of the existing methods for hydrogen isotope separation—such as distillation, exchange reactions, electrolysis, etc.—depend on small differences in the average behavior of molecules. This results in a small separation factor so that many stages are required. Compared to these methods, utilizing quantum-induced kinetic selectivity combined with the equilibrium selectivity of microporous materials will be less complex and economically more viable.

Acknowledgment. This research has been supported by a grant from the Australian Research Council, under the Discovery Scheme.

References and Notes

(1) Wang, Q.; Johnson, J. K.; Broughton, J. Q. *Mol. Phys.* **1996**, *89*, 1105–1119.
(2) Rick, S. W.; Lynch, D. L.; Doll, J. D. *J. Chem. Phys.* **1993**, *99*, 8183–8193.
(3) Pavese, M.; Voth, G. A. *Chem. Phys. Lett.* **1996**, *249*, 231–236.
(4) Hone, T. D.; Voth, G. A. *J. Chem. Phys.* **2004**, *121*, 6412–6422.
(5) Miura, S.; Okazaki, S.; Kinugawa, K. *J. Chem. Phys.* **1999**, *110*, 4523–4532.
(6) Beenaker, J. J. M.; Borman, V. D.; Krylov, S. Y. *Chem. Phys. Lett.* **1995**, *232*, 379–382.
(7) Wang, Q. Y.; Challa, S. R.; Sholl, D. S.; Johnson, J. K. *Phys. Rev. Lett.* **1999**, *82*, 956–959.
(8) Challa, S. R.; Sholl, D. S.; Johnson, J. K. *Phys. Rev. B* **2001**, *63*, 245419–2001.
(9) Hattori, Y.; Tanaka, H.; Okino, F.; Touhara, H.; Nakahigashi, Y.; Utsumi, S.; Kanoh, H.; Kaneko, K.; et al. *J. Phys. Chem. B* **2006**, *110*, 9764–9767.
(10) Garberoglio, G.; DeKlavon, M. M.; Johnson, J. K. *J. Phys. Chem. B* **2006**, *110*, 1733–1741.
(11) Kotoh, K.; Nishikawa, T.; Kashio, Y. *J. Nucl. Sci. Technol.* **2002**, *39*, 435–441.
(12) Kumar, A. V. A.; Bhatia, S. K. *Phys. Rev. Lett.* **2005**, *95*, 245901.

(13) Kumar, A. V. A.; Jobic, H.; Bhatia, S. K. *J. Phys. Chem. B* **2006**, *110*, 16666–16671.

(14) Zhao, X. B.; Villar-Rodil, S.; Fletcher, A. J.; Thomas, K. M. *J. Phys. Chem. B* **2006**, *110*, 9947–9955.

(15) Chu, X-Z.; Zhou, Y. P.; Zhang, Y. Z.; Su, W.; Sun, Y.; Zhou, L. *J. Phys. Chem. B* **2006**, *110*, 22596–22600.

(16) Richardson, J. W.; Smith, J. V.; Pluth, J. L. *J. Phys. Chem.* **1990**, *94*, 3365–3367.

(17) Feynman, R. P. ; Hibbs, A. R. *Quantum Mechanics and Path Integrals*; McGraw-Hill: New York, 1965.

(18) June, R. L.; Bell, A. T.; Theodorou, D. N. *J. Phys. Chem.* **1991**, *95*, 8866–8878.

(19) Eyring, H. *J. Chem. Phys.* **1935**, *3*, 107–115.

(20) Anderson, J. B. *J. Chem. Phys.* **1973**, *58*, 4684–4692.

(21) Wert, C. A. *Phys. Rev.* **1950**, *79*, 601–605.

(22) Ruthven, D. M.; Derrah, R. I. *J. Chem. Soc. Faraday. Trans. 1* **1972**, *68*, 2332–2343.

(23) Kopelevich, D. I.; Chang, H.-C. *J. Chem. Phys.* **2001**, *114*, 3776–3789.

(24) Demontis, P.; Suffriti, G. B.; Fois, E. S.; Quartieri, S. *J. Phys. Chem.* **1992**, *96*, 1482–1490.

(25) Fritzsche, S.; Wolfsberg, M.; Haberlandt, R.; Demontis, P.; Suffritti, G. B.; Tilocca, A. *Chem. Phys. Lett.* **1998**, *296*, 253–258.

(26) Evans, D. ; Morris, G. P. *Statistical Mechanics of Nonequilibrium Liquids*; Academic Press: London, 1990.

(27) Beerdsen, E.; Smit, B.; Dubbeldam, D. *Phys. Rev. Lett.* **2004**, *93*, 248301.

(28) Widom, B. *J. Chem. Phys.* **1963**, *39*, 2808–2812.

(29) Frenkal D. ; Smit, B. *Understanding Molecular Simulations*; Academic Press: London, 2002.

JP8015358